Applied Thermal Engineering 290 (2026) 129932

Contents lists available at ScienceDirect

Applied Thermal Engineering

journal homepage: www.elsevier.com/locate/apthermeng

Research Paper

Development and calibration of an original 1D scavenging model for opposed-piston two-stroke engines

Emiliano Pipitone [a,b,*], Marco Giannone [b]

[a] Department of Engineering, University of Palermo, 90133 Palermo, Italy
[b] National Sustainable Mobility Center (Centro Nazionale per la Mobilità Sostenibile-CNMS), 35122 Padova, Italy

ARTICLE INFO

Keywords:
Two stroke internal combustion engine
Opposed piston engine
thermodynamic simulation
1D modelling
Uniflow scavenging
Longitudinal scavenging

ABSTRACT

The use of hydrogen in internal combustion engines may pose several issues and concerns, above all if, with the aim to reach near zero emissions, the adoption of lean mixtures is considered: in this condition, the engine power density may reveal too low and seriously limit the implementation in sport cars. A possible solution to this problem may be offered by the 2 stroke engines, above all in the opposed piston configuration, whose characteristic of high-power density may allow sport car requirements to comply with hydrogen fuel. As widely known, the first step for performance verification and optimization is represented by thermodynamic simulations, usually performed with an in-cylinder zero-dimensional (0D) approach coupled with a two-zones combustion model. Opposed-piston two-stroke (OP2S) engines feature a longitudinal scavenging process that strongly influences overall performance and emissions. Conventional scavenging modelling approaches rely on 0D formulations fundamentally based on blending the perfect mixing and the perfect displacement models, or on the "scavenging curve" (also called "scavenging profile") obtained by means of extensive three-dimensional computational fluid dynamics (3D CFD) simulations. These approaches however cannot capture the axial evolution of the longitudinal gas exchange typical of OP2S. This paper presents an innovative one-dimensional (1D) scavenging model developed to introduce axial resolution in the scavenging process of OP2S engine while remaining compatible with system-level simulations. The proposed model is fully specified through explicit governing equations and introduces axial resolution through a continuous dilution-front formulation, avoiding the need for proprietary 1D toolchains and CFD-derived closure quantities. The model couples a full-cycle thermodynamic solver, which provides the in-cylinder state at port opening, with a 1D two-zone dilution formulation describing the interaction between fresh charge and residual gases. The model proposed only requires the identification of two scalar parameters to correctly predict scavenging parameters. The model calibration was performed using experimental scavenging and trapping-efficiency data from a reference OP2S engine, by minimizing the mean-square error across multiple intake-pressure levels. As an overall result, the model demonstrated accurate reproduction of measured scavenging and trapping efficiency.

Symbols and abbreviations

a	Wiebe function efficiency factor
A_{piston}	Piston crown surface area (mm^2)
B	Cylinder bore (mm)
BDC	Bottom Dead Centre
CA	Crank Angle
CAD	Crank Angle Degree
C_d	discharge coefficient
c_p	specific heat at constant pressure (J/Kg-K)
$c_{p,a}$	fresh charge specific heat at constant pressure (J/Kg-K)
$c_{p,a0}$	intake ambient specific heat at constant pressure (J/Kg-K)
$c_{p,res}$	residual gases specific heat at constant pressure (J/Kg-K)
$G_{a,out}$	fresh charge exhaust flow (Kg/s)
G_{in}	intake mass flow (Kg/s)
G_{out}	exhaust mass flow (Kg/s)
$G_{res,out}$	residual gases exhaust flow (Kg/s)
$h_1(\vartheta)$, $h_2(\vartheta)$	port height (mm)
H_i	Fuel lower heating value (MJ/Kg)
h_w	convective heat transfer coefficient (J/m^2K)
i_{in}	inlet total specific enthalpies (J/Kg)

(*continued on next column*)
(*continued*)
(*continued on next page*)

* Corresponding author at: Department of Engineering, University of Palermo, 90133 Palermo, Italy.
E-mail address: emiliano.pipitone@unipa.it (E. Pipitone).

https://doi.org/10.1016/j.applthermaleng.2026.129932
Received 13 October 2025; Received in revised form 12 January 2026; Accepted 22 January 2026
Available online 24 January 2026

(*continued*)

i_{out}	outlet total specific enthalpies (J/Kg)
k	Isentropic coefficient (J/Kg-K)
k_a	fresh charge isentropic coefficient
k_{res}	residual gases isentropic coefficient
L	total length of the cylinder (mm)
m	Wiebe function shape coefficient
m_a	fresh charge mass (Kg)
$m_{a,scavenged}$	fresh charge scavenged mass (Kg)
$m_{a,trapped}$	fresh charge trapped mass (Kg)
MAP	intake Manifold Absolute Pressure (bar)
MFB	Mass Fraction Burnt
m_{fuel}	fuel mass (Kg)
m_{H2}	hydrogen mass (Kg)
m_{H2O}	water mass (Kg)
m_{N2}	nitrogen mass (Kg)
m_{O2}	oxygen mass (Kg)
m_{res}	residual gases mass
MSE	Mean Square Error
m_{tot}	total in-cylinder mass (Kg)
n	engine speed (rpm)
OP2S	Opposed Pistons 2 stroke
OPE	Opposed Pistons Engine
p	pressure (bar)
p_0	upstream nozzle total pressure (bar)
p_e	exhaust pressure (bar)
Q	total heat received by the in-cylinder gas (J)
Q_{wall}	heat transferred to the wall (J)
Q_{wall}	heat released by the combustion (J)
r	crank radius (mm)
R'	specific gas constant (J/Kg-K)
R'_a	fresh charge gas constant (J/Kg-K)
R'_{res}	residual gases constant (J/Kg-K)
S	stroke (mm)
S_{wall}	wall surface area (mm^2)
T	temperature (K)
T_a	intake ambient temperature (K)
T_a	fresh charge temperature (K)
TDC	Top Dead Centre
T_{res}	residual gases temperature (K)
T_{wall}	wall temperature (K)
V	displacement (L)
V_1, V_2	swept volume by each piston (L)
V_a	fresh charge volume (L)
V_c	geometric clearance volume (L)
V_{res}	residual gases volume (L)
V_{tot}	total volume (L)
x	scavenging model coordinate (mm)
X_{H2}	hydrogen mass fraction
X_{H2O}	water mass fraction
X_{N2}	nitrogen mass fraction
X_{O2}	oxygen mass fraction
x_{s1}, x_{s2}	piston position (mm)
y	delivery ratio
ℓ_1, ℓ_2	port coverage ratio
$\Delta\vartheta_{burn}$	combustion duration (deg)
η_{ls}	trapping efficiency
ϑ	crank angle (deg)
ϑ_a	max intake port opening angle (deg)
ϑ_b	max exhaust port opening angle (deg)
$\vartheta_{e,c}$	exhaust port closing angle (deg)
ϑ_i	start of combustion angle (deg)
$\vartheta_{i,c}$	intake port closing angle (deg)
ϑ_{inj}	fuel injection duration (deg)
$\vartheta_{i,s}$	start of intake fresh charge flow (deg)
ϑ_s	crank angle offset (deg)
λ_v	scavenging efficiency
μ	connecting rod-to-crank radius ratio
ρ_g	geometric compression ratio
ρ_0	upstream nozzle density (Kg/m^3)
ρ_a	fresh charge density inside the cylinder (Kg/m^3)
ρ_{eff}	effective compression ratio
ρ_{res}	residual gases density (Kg/m^3)
ρ_s	gas density at the exhaust port (Kg/m^3)
φ	slope variation constant (1/Kg-mm)
χ_a	fresh charge volumetric fraction
ψ	scavenging model slope (1/mm)
ψ_0	initial scavenging model slope (1/mm)
ω	angular velocity (deg/s)

1. Introduction

The climate crisis of recent decades led regulatory authorities to issue increasingly stringent emissions regulations. This has resulted in increased efforts by the scientific community to search for innovative solutions to comply with such standards [1]. The use of green hydrogen in internal combustion engines by the automotive industry therefore represents a valid alternative to traditional fuels. These engines have shown excellent potential in terms of emissions, achieving nearly zero emissions when operating with very lean mixtures: although the absence of carbon in the combustion process does not eliminate all pollutants, maintaining a lean mixture significantly reduces combustion temperatures, resulting in an almost complete suppression of nitrogen oxide (NO_x) formation [2]. However, the combination of high air-to-fuel ratios and the low density of hydrogen results in low specific power output in conventional four-stroke engines, making it unattractive for automotive applications. A solution to this issue can be found in the use of opposed-piston two-stroke (OP2S) engines [3]. This engine architecture was introduced in the 1950s by the German engineer Witting, who developed one of the first prototypes powered by gas [4]. It was subsequently employed in various industrial applications, before falling into disuse in the 1970s due to increasingly strict pollution regulations. More recently, thanks to technological advances in materials, fuelling systems, and modern analytical tools, companies such as FEV, Eco Motors, and Achates Power have demonstrated the suitability of this engine configuration in present-day applications [5–10]. One of the defining features of opposed-piston two-stroke engines is their unidirectional scavenging process, which is considered among the most efficient for two-stroke engines [11]. The scavenging process consists of three main phases: the blowdown phase, in which the opening of the exhaust port rapidly reduces the internal cylinder pressure by discharging residual combustion gases; the scavenging phase, during which the residual gases are progressively replaced by fresh charge; and finally, the blow-fill phase, in which an additional amount of fresh air is introduced—typically through supercharging systems—until the intake port is fully closed [12]. The performance of this process is assessed through specific parameters such as trapping efficiency, scavenging efficiency, and delivery ratio, which are fundamental to quantifying the amount of fresh air retained in the cylinder and predicting the engine's overall performance [11,13]. When the performances of 2 stroke engines are evaluated by means of zero-dimensional simulations, the perfect mixing model is frequently adopted for the calculation of scavenging and trapping efficiency. However, when the scavenging process is longitudinal (i.e. the gas mainly flows from bottom to top of the cylinder, or vice-versa) or the cylinder length is notable with respect to the bore, the perfect mixing approach becomes quite unreliable; as example Fig. 1 shows the scavenging efficiency experimentally measured on an opposed piston 2S engine [14], compared to prefect mixing and prefect displacement models predictions; as can be observed, when uniflow processes are involved, the perfect mixing (which assumes a continuous and uniform mixing of fresh gas and residual gas) strongly underestimate the scavenging performances, which instead reveals consistent with a perfect displacement process.

Relevant 0D models, including blended formulations of perfect mixing and perfect displacement as well as three-zone or multi-stage schemes, have been proposed in the literature and provide useful global estimates of the scavenging process in two-stroke engines [14–19]. However, their intrinsic lack of axial resolution limits their applicability to high stroke-to-bore ratio geometries involved in longitudinal scavenging and, above all, in OP2S engines; moreover these models rely on the calibration of several empirical parameters (up to five in the case of uniflow scavenging) further undermining their predictive capability, leading to a systematic overestimation of scavenging performance compared with experimental data [20].

In the broader two-stroke literature, one-dimensional (1D)

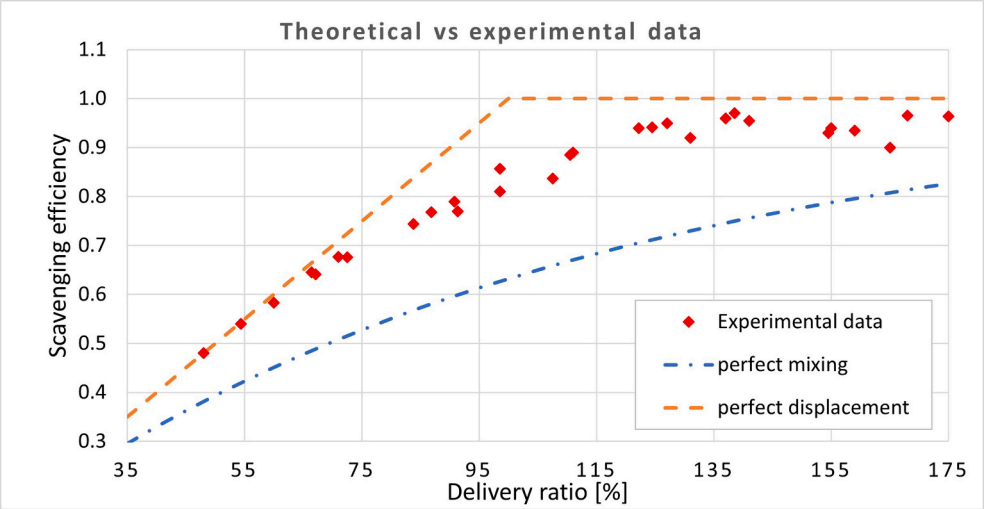

Fig. 1. Scavenging efficiency in a 2-stroke opposed-piston engine: theoretical vs experimental data [14].

commercial tools such as GT-POWER and Ricardo WAVE (which provide robust gas-dynamics solvers but require proprietary toolchains and model structures that are not reproducible from the open literature) have been frequently employed to simulate gas flows in the intake and exhaust ducts for engine design and performance optimisation: in these studies, however, the in-cylinder scavenging process has been described by well-known 0D models [21] or by means of the "scavenging curve" (also referred to as "scavenging profile") obtained by means of extensive three-dimensional computational fluid dynamics (3D CFD) simulations [22].

The same approach has been followed in the field of OP2S engines, where commercial 1D simulation platforms (GT-POWER, AVL BOOST) have been coupled to 0D scavenging models based on blended formulations of perfect mixing and perfect displacement [23,24]. It is also worth highlighting that, since these commercial platforms do not support the opposed-piston cylinders as a native configuration, the OP2S engine has been implemented by means of "equivalent-cylinder" representations or customised piston-motion profiles, which further reduces portability outside the original software environment. In these mixed 1D–0D setups, 3D CFD simulations are frequently employed to calibrated discharge/flow coefficients and/or synthetic scavenging profiles, thus increasing the development effort and limiting the predictive robustness when extrapolating across operating conditions. 1D tools implementation linked to CFD simulations have been also used to supply initial/boundary conditions for the scavenging phase or to identify mixing/entrainment coefficients. This approach makes necessary turbulence-related quantities [25] (e.g., turbulence intensity or length scales, swirl/tumble metrics, or eddy-viscosity surrogates) that are not directly available from a 0D cycle solver and require time-consuming calibration. In practice, these 1D frameworks are often co-simulated or tuned by means of 3D CFD [26].

Dealing specifically with OP2S engines, high-fidelity studies show that 3D CFD resolves jet development and in-cylinder mixing and is therefore widely used to investigate the effects of port geometry (height, angle) and flow organization (e.g., swirl level) on short-circuiting and residual-gas distribution [22–27]. A representative example is the work by Yang et al. [28], where the scavenging process of the an opposed-piston diesel engine is characterized through a "scavenging curve" pre-determined performing several 3D CFD simulations; although highly informative, this approach still relies on CFD to generate the core scavenging dataset. As widely seen, however, the computational cost of CFD often forces iterative coupling with 1D commercial tools, limiting rapid sweeps or real-time use. Accordingly, CFD is often reserved to a limited set of operating points and used to build or validate simplified models, rather than to cover wide parametric maps at system level [14,22,23].

Despite the extensive literature on 0D scavenging correlations, on the implementation of commercial 1D tools and on 3D CFD investigations, the open literature still lacks a stand-alone and fully explicit 1D model suitable for predictive simulations of in-cylinder uniflow scavenging processes and that can be directly implemented in a system-level environment and coupled transparently with a custom full-cycle 0D thermodynamic solver, without requiring proprietary 1D software access and without relying on CFD-derived closure quantities or CFD-generated scavenging profiles [14,22–27]. This gap is especially relevant for hydrogen-fuelled OP2S studies, where fast, repeatable, and transparent simulation tools are needed to support early-stage architecture screening and scavenging-system assessment over multiple operating conditions. This lack motivated the authors to explore the application of the 1D approach, which add an axial degree of freedom without the cost of full 3D CFD, to study and describe the scavenging process of OP2S engines. This paper presents an original 1D scavenging model for OP2S engines that is fully specified in the manuscript through a compact set of explicit governing equations and can be directly implemented in system-level simulation environments (e.g., MATLAB/Simulink) without requiring CFD coupling or CFD-derived closure quantities. The fresh-charge penetration is represented through a linear axial dilution front along a continuous cylinder coordinate and is coupled to the full-cycle 0D thermodynamic solver via mass and energy conservation. Compared with commonly adopted multi-zone approaches, which describe stratification through lumped control volumes and typically involve additional empirical mixing parameters, the proposed formulation provides an explicit axial degree of freedom while keeping the calibration effort minimal. In particular, only two scalar parameters (ψ_0 and φ) are required. The model is calibrated using experimental scavenging and trapping-efficiency data available for the opposed-piston diesel engine developed by the Beijing Institute of Technology [14], and its predictive capability is assessed over multiple intake-pressure levels. The proposed framework is intended to enable fast parametric studies and design-space exploration of OP2S scavenging at system level, while maintaining full transparency of the governing equations and a minimal calibration burden.

2. Engine models

The newly proposed scavenging model has been developed within a full-cycle zero-dimensional thermodynamic model of a two-stroke opposed piston engine, encompassing compression, combustion, and

expansion phases. The necessary initial thermodynamic conditions for the scavenging process simulation were hence obtained as the finishing gas condition at the end of the full-cycle simulation. Both scavenging model and full-cycle simulation model were implemented in Matlab Simulink environment. The model was integrated using the variable-step ode45 solver. At the transition between the 0D full-cycle formulation and the 1D scavenging formulation, small discontinuities were occasionally observed in the in-cylinder pressure signal used by the nozzle-flow relations for the intake and exhaust mass-flow calculations. To prevent non-physical spikes in the computed mass flow rates and ensure robust numerical integration, a saturation/limiting block was applied to the in-cylinder pressure input of the nozzle-flow equations. With this approach, no solver divergence was encountered over the investigated operating conditions. The simulations were run on a machine equipped with an AMD Ryzen 97940HS (up to 5.2 GHz) and 16 GB DDR5 RAM. As convergence criterion, each simulated in-cylinder pressure cycle was compared to the previous one, computing the pressure difference at each crank angle position (360 values for each cycle). The maximum value of this pressure difference was assumed as the convergence parameter, and the simulation result was considered as the final solution when the maximum pressure difference revealed to be lower than 100 Pa. The simulation time was measured in MATLAB using a tic/toc timing logic. On average, the solution reached periodic convergence after 6 complete simulated engine cycles and the average clock time per simulated cycle was 21.2 s.

2.1. Engine geometry

Fig. 2 reports a simple representation of the OP2S engine geometry considered in this paper. As can be seen, the single cylinder is endowed of two pistons, each one connected to its crank mechanism. The intake and exhaust ports are located on the two opposite sides of the cylinder, thus producing a longitudinal scavenging process, also known as uni-directional flow (or uniflow). In the assumed geometric scheme, the intake-side (1) is positioned on the left, while the exhaust-side (2) is on the right.

The instantaneous in-cylinder volume can be evaluated, as function of the crank angular position θ, as the difference between the total volume inside the cylinder V_{tot} and the volume swept by each piston:

$$V(\theta) = V_{tot} - V_1(\theta) - V_2(\theta + \theta_s) \tag{1}$$

$$V_{tot} = 2 \cdot \frac{\pi B^2}{4} \cdot S + V_c \tag{2}$$

where B is the cylinder bore, S is the piston stroke and V_c is the geometric clearance volume (i.e. the in-cylinder volume portion which is not crossed by the two pistons). Subscripts 1 and 2 refer to the intake-side and exhaust-side respectively, while θ_S represents the crank-angle phase offset between the two crank mechanisms. The volume $V_i(\theta)$ swept by each piston can be calculated using the standard trigonometric formulation derived for crank-slider kinematics:

$$x_{s1}(\theta) = r\left[1 - cos(\theta) + \frac{1}{\mu}\left(1 - \sqrt{1 - \mu^2 sin^2(\theta)}\right)\right] \tag{3}$$

$$x_{s2}(\theta) = r\left[1 - cos(\theta + \theta_s) + \frac{1}{\mu}\left(1 - \sqrt{1 - \mu^2 sin^2(\theta + \theta_s)}\right)\right] \tag{4}$$

$$V_i(\theta) = A_{piston} \cdot x_{s,i}(\theta) = \frac{\pi B^2}{4} \cdot x_{s,i}(\theta) \tag{5}$$

Being $x_{s,i}(\theta)$ the position of the i-piston, μ the connecting rod-to-crank radius ratio and A_{piston} the pistons surface area. In OP engines, intake and exhaust ports are machined into the cylinder wall and are uncovered by the reciprocating motion of the pistons, eliminating the need for valves. Intake ports are specifically inclined with respect to the radial direction (typically between 10° and 20°) to induce a swirling motion inside the combustion chamber, enhancing air-fuel mixing and promoting more rapid and uniform combustion [26]. With reference to the generic the i-port, $h_i(\theta_i)$ is its instantaneous axial height (the maximum value $h_{i,max}$ is reached when the port is completely open), β_i is the circumferential port coverage ratio and A_i the ports areas modelled as a function of the pistons position; it derives that, for the intake port is:

$$A_1 = \pi \cdot B \cdot \beta_1 \cdot h_1(\theta) \tag{6}$$

$$\begin{cases} h_1(\theta) = x_{s1}(\theta_{i,c}) - x_{s1}(\theta) \\ 0 \le h_1(\theta) \le h_{1,max} \\ h_{1,max} = x_{s1}(\theta_{i,c}) - x_{s1}(\theta_a) \end{cases} \tag{7}$$

where θ_a represents the crank angle at which the intake port is fully open, whereas $\theta_{i,c}$ corresponds to the angle at which the intake port is fully closed by the piston. As regards the exhaust port, similar equation may be used:

$$A_2 = \pi \cdot B \cdot \beta_2 \cdot h_2(\theta) \tag{8}$$

$$\begin{cases} h_2(\theta) = x_{s2}(\theta_{e,c}) - x_{s2}(\theta) \\ 0 \le h_2(\theta) \le h_{2,max} \\ h_{2,max} = x_{s2}(\theta_{e,c}) - x_{s2}(\theta_b) \end{cases} \tag{9}$$

θ_b denotes the crank position when the exhaust port is fully open, while $\theta_{e,c}$ indicates the crank position for the complete closure. When dealing with opposed-piston engines, it is common to refer to the effective compression ratio, ρ_{eff}. This differs from the geometric compression ratio, ρ_g, due to the presence of intake and exhaust ports, as well as to the

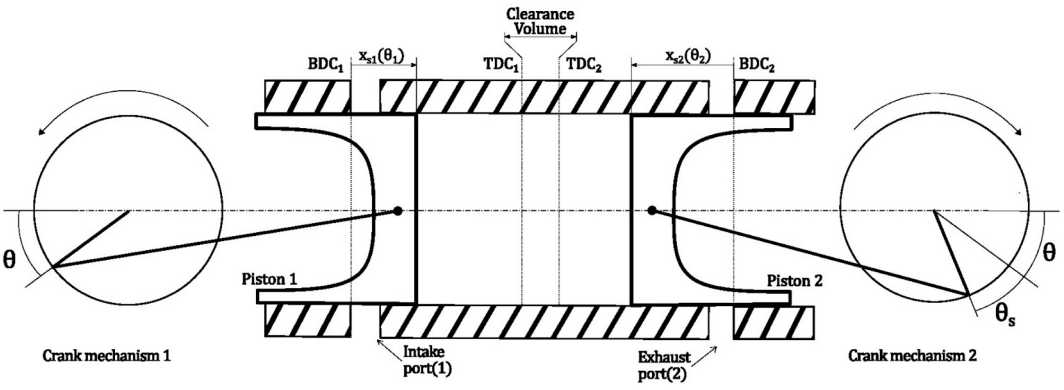

Fig. 2. Schematic representation of the geometry adopted for the 2 strokes opposed piston engine.

crankshaft phase difference between the two pistons. The presence of intake and exhaust ports implies that no actual compression occurs if both ports are not completely closed. Consequently, the compression process starts later with respect to the BDC (as therefore happens in four strokes engines due to the inlet valve closure delay), resulting in a lower effective compression ratio. Additionally, the crankshaft phase offset θ_s between the two pistons influences the minimum in-cylinder volume achieved during the cycle, thus further modifying the effective compression ratio ρ_{eff} compared to the geometrical ratio ρ_g.

The geometry parameters adopted in this paper are based on the opposed-piston engine developed at the Beijing Institute of Technology presented by Xie et al. [14,22], since it provides some experimental measurements related to the scavenging process that have been employed in the present paper for the identification of the model parameters.

Although the geometry implemented in the model reproduces the main dimensional features of Xie's OP2S [14,22], including cylinder volume and effective compression ratio, minor differences in the overall layout required a tuning of port heights and timings: the curves in Fig. 3 represent the adopted port areas as function of crank position. These adjustments were necessary to ensure that the resulting effective compression ratio and the overall port area remained close to those of the reference engine, maintaining physical consistency with the benchmark configuration. The numerical models are both based on the engine parameters summarized in Table 1.

Table 1
Main engine parameters.

Parameter	Symbol	Value	Unit
Bore	B	100	mm
Stroke	S	110	mm
Displacement	V	1.8	L
Engine speed	N	1200	rpm
Crank-angle offset between pistons	θ_s	9.7	deg
Connecting rod-to-crank radius ratio	μ	0.290	–
Geometric compression ratio	ρ	22	–
Effective compression ratio	ρ_{eff}	15.80	–
Intake port closing angle	$\theta_{i,c}$	46	deg aBDC
Max intake port opening angle	θ_a	0	deg aBDC
Max exhaust port opening angle	θ_b	9.7	deg bBDC
Exhaust port closing angle	$\theta_{e,c}$	44.3	deg aBDC
Max intake port height	$h_{1,max}$	21.0	mm
Max exhaust port height	$h_{2,max}$	28.0	mm
Intake port coverage ratio	β_1	0.754	–
Exhaust port coverage ratio	β_2	0.724	–

2.2. Thermodynamic model

To determine the key thermodynamic properties of the engine cycle, the authors followed the approach usually adopted for zero-dimensional thermodynamic simulations in internal combustion engines [29]. This methodology is based on the first law of thermodynamics and the mass conservation principle, both expressed as functions of the crank angle and applied to the control volume of the cylinder:

$$\frac{dp}{d\theta} = \frac{k-1}{V(\theta)} \cdot \left[\frac{\delta Q}{d\theta} - \frac{k}{k-1} \cdot p \cdot \frac{dV}{d\theta} + \frac{G_{in} \cdot i_{in} - G_{out} \cdot i_{out}}{\omega} \right] \tag{10}$$

$$\frac{dm_{tot}}{d\theta} = \frac{G_{in} - G_{out}}{\omega} \tag{11}$$

where:

- m_{tot} is the instantaneous in-cylinder mass
- G_{in} and G_{out} are the mass flow rates entering and leaving the cylinder
- θ is the crank angle
- ω is the angular velocity of the engine
- δQ is the net heat received by the in-cylinder gas
- p is the in-cylinder pressure
- V is the instantaneous in-cylinder volume
- i_{in}, i_{out} are the total specific enthalpies of the incoming and outgoing flows
- T is the average in-cylinder gas temperature
- k is the ratio of specific heats, dependent on gas temperature and composition

2.2.1. Net heat introduction

The net heat received by the gas δQ is comprised of two main components, the heat transferred to the cylinder walls δQ_{walls} and the gross heat released by the combustion δQ_{comb}:

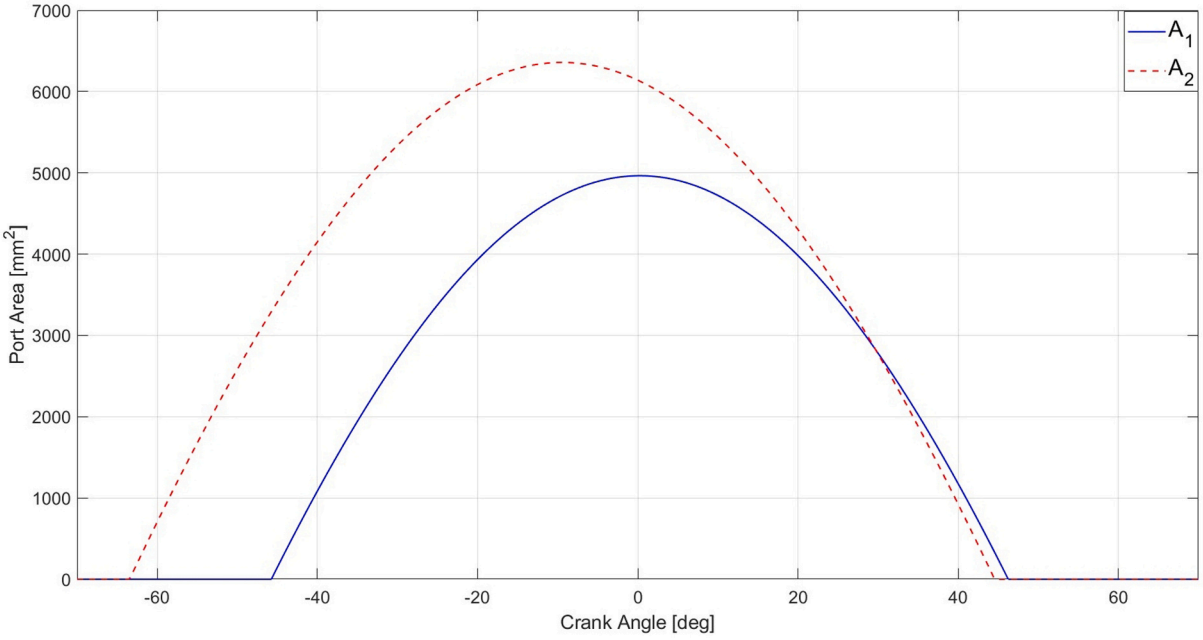

Fig. 3. Ports area as function of crack position (referred to the BDC of piston 1).

$$\delta Q = \delta Q_{comb} + \delta Q_{walls} \tag{12}$$

The elementary heat transferred to the wall during the elementary crank rotation $d\theta$ has been evaluated as:

$$\delta Q_{walls} = h_w \cdot S_{wall} \cdot (T_{wall} - T) \cdot \frac{d\theta}{\omega} \tag{13}$$

where:

- h_w is the convective heat transfer coefficient, calculated using the Woschni correlation [30]
- S_{wall} is the in-cylinder surface area
- T and T_{wall} are the gas and wall temperatures respectively

It is worth noting that, even if not expressly developed for two stroke engines, the Woschni model is currently the most widely adopted for instantaneous in-cylinder wall heat transfer calculation in zero-dimensional simulations [8,11,12,17,23].

As instead regards the heat released by the combustion:

$$\delta Q_{comb} = H_i \cdot m_{fuel} \cdot \left(\frac{dMFB}{d\theta}\right) d\theta \tag{14}$$

where:

- H_i is the lower heating value of the fuel (hydrogen in this case)
- m_{fuel} is the injected fuel mass
- $\frac{dMFB}{d\theta}$ is the mass fraction burn rate

As already mentioned, the main focus of this paper is the development and validation of a new, one-dimensional scavenging model for 2 strokes opposed piston engines; the simulation of the entire cycle has not the claim to give a reliable prediction of the engine performance but the only purpose to fairly produce the residual gas that interacts with the fresh charge during the scavenging process; according to this consideration, the authors adopted the simple, non-predictive, mass fraction burn (MFB) model widely adopted for such kind of simulations, i.e. the Wiebe function:

$$MFB(\theta) = 1 - e^{\left[-a \cdot \left(\frac{\theta - \theta_i}{\Delta\theta_{burn}}\right)^{m+1}\right]} \tag{15}$$

Whose derivative is:

$$\frac{dMFB}{d\theta} = a \cdot \frac{(m+1)}{\Delta\theta_{burn}} \cdot \left(\frac{\theta - \theta_i}{\Delta\theta_{burn}}\right)^m e^{\left[-a\left(\frac{\theta - \theta_i}{\Delta\theta_{burn}}\right)^{m+1}\right]} \tag{16}$$

Being a and m the efficiency factor and the shape coefficient of the Wiebe function, θ_i the crank angle at the start of the combustion, and $\Delta\theta_{burn}$ the combustion duration (in crank angles). The values adopted for the combustion and the wall heat transfer models are summarized in Table 2.

2.2.2. Working fluid properties

The accurate modelling of the thermodynamic cycle requires a proper representation of the working fluid, which in the present case is treated as a gas mixture. The key thermophysical properties of interest, such as specific heat at constant pressure c_p, specific gas constant R', and the isentropic exponent k, are not assumed constant but considered to vary dynamically as functions of temperature and chemical composition. For each parameter, a mass based averaging calculation was followed taking into consideration all the chemical species composing the mixture. The constant pressure specific heat of the mixture was then computed as:

$$c_{p_{mix}} = \sum_i c_{p,i} \cdot X_i \tag{17}$$

where X_i represents the mass fraction of the i-species and $c_{p,i}$ its constant pressure specific heat. A similar formulation was adopted for the computation of the gas constant R'.

$$R'_{mix} = \sum_i R'_i \cdot X_i \tag{18}$$

It derives that isentropic exponent k_{mix} of the mixture can be obtained as:

$$k_{mix} = \frac{c_{p_{mix}}}{c_{p_{mix}} - R'_{mix}} \tag{19}$$

The calculation of the mass fractions X_i of each single chemical species inside the cylinder was performed following its mass variation inside the cylinder:

$$m_i = \int \frac{G_{i,in} - G_{i,out}}{\omega} d\theta \pm \int \left(\frac{dm_i}{d\theta}\right) d\theta \tag{20}$$

The first term accounts for the net contribution due to the difference between the incoming and the outgoing flows of species i through the ports; the second term, instead, accounts for the change caused by the combustion, if the generic species i is involved in the air-fuel reaction. Air was modelled as a binary mixture composed of oxygen and nitrogen, whose incoming mass flow rates were computed as:

$$G_{i,in} = G_{in} \cdot X_{i,air} \tag{21}$$

Assuming dry air with a molar composition of 21% O_2 and 79% N_2, and molar masses of 31.9988 g/mol and 28.0134 g/mol (for O_2 and N_2 respectively), the resulting mass fractions are:

$$X_{O_2\,air} = 0,233 \qquad X_{N_2\,air} = 0,767$$

Hydrogen was supposed to be introduced thorough direct injection over a specified crank angle interval θ_{inj}. The total injected mass of hydrogen was hence given by:

$$m_{H_2,in} = \int_{\theta_{inj}} G_{H_2}(\theta) d\theta \tag{22}$$

where the G_{H2} represents the injector hydrogen mass flow.

The rates of variation of oxygen, hydrogen and water vapor during the combustion process were deduced by assuming a complete reaction; as a result, the rate of formation of water vapor and the rate of reaction of oxygen were both computed based on the rate of reaction of hydrogen:

$$\frac{dm_{H_2O}}{d\theta} = -9 \cdot \frac{dm_{H_2}}{d\theta} \tag{23}$$

$$\frac{dm_{O_2}}{d\theta} = 8 \cdot \frac{dm_{H_2}}{d\theta} \tag{24}$$

The hydrogen reaction rate, in turn, was simply related to the fuel burn rate:

$$\frac{dm_{H_2}}{d\theta} = m_{H_{2,in}} \cdot \frac{dMFB}{d\theta} \tag{25}$$

The above relations allow defining the governing equations for the time evolution of each species' mass fraction X_i. The accuracy of the

Table 2
Wall heat transfer and combustion model parameters.

Parameter	Symbol	Value	Unit
Average wall temperature	T_w	500	K
Wiebe efficiency factor	a	5	–
Wiebe shape coefficient	m	2	–
Combustion duration	$\Delta\theta_{burn}$	50°	deg
Start of combustion	θ_i	22.5°	deg bTDC
Lower Heating Value (hydrogen)	H_i	120	MJ/kg

model was further improved by including also the temperature dependence of the specific heat. This dependence is described through polynomial expressions obtained from the NIST database [31], enabling realistic computation of c_p across the engine's full operating temperature range. This aspect is particularly relevant during combustion and expansion, where steep temperature gradients significantly influence internal energy and pressure evolution.

2.3. Inlet and exhaust mass flow

The mass flow rates G_{in} and G_{out} through the ports were computed using nozzle flow equations, both for the subcritical and the critical conditions, endowed of proper discharge coefficient for real mass flow evaluation:

$$G = C_d \cdot A(\theta) \sqrt{\frac{2k}{k-1} \cdot p_0 \cdot \rho_0 \cdot \left[\left(\frac{p}{p_0}\right)^{\frac{2}{k}} - \left(\frac{p}{p_0}\right)^{\frac{k+1}{k}} \right]} \text{ for subcritical flow, i.e. } \frac{p}{p_0} > \left(\frac{2}{k+1}\right)^{\frac{k}{k-1}} \tag{26}$$

$$G = C_d \cdot A(\theta) \sqrt{p_0 \cdot \rho_0 \cdot k \cdot \left(\frac{2}{k+1}\right)^{\frac{k+1}{k-1}}} \text{ for critical flow, i.e. } \frac{p}{p_0} \leq \left(\frac{2}{k+1}\right)^{\frac{k}{k-1}} \tag{27}$$

The variables with subscript "*0*" refer to stagnation conditions upstream of the nozzle, C_d is the discharge coefficient, $A(\theta)$ is the nominal flow area, function of crank position θ, and ρ is the gas density. To compute the mass flow through the exhaust ports, it is necessary to evaluate the average thermodynamic properties of the gas species exiting the cylinder. Specifically, the average density ρ_s and the average isentropic exponent k_s of the gas mixture (composed by fresh charge and residual gas) must be determined, as they are used to calculate the outflow rate from the cylinder. This calculation will be discussed further on. Table 3 reports the values adopted for the parameters involved in the calculation of mass flows.

2.4. Scavenging model

As already mentioned, in opposed-piston engines, both intake and exhaust ports are integrated directly into the cylinder structure at its opposite ends. This configuration results in a scavenging dynamic that is predominantly axial and is usually referred to as unidirectional flow (uniflow) or longitudinal scavenging. As previously discussed, the "perfect mixing model", frequently adopted for 2-stroke engines, reveals quite inadequate to describe the uniflow scavenging process of an opposed piston engine, giving, as a result, a an unreliable prediction of the scavenging efficiency, as shown in Fig. 1. This led the authors to develop the original simple one-dimensional scavenging model here presented. The following considerations and assumptions guided the development of the model: when the fresh charge enters through the intake ports, it starts a simultaneous action of mixing and displacement of the residual gas toward the exhaust ports (located at the opposite end); at the beginning of the scavenging process, the fresh charge admitted into the cylinder accumulates near the intake ports, and the outgoing flow involves only the residual gas; during the scavenging process, the fresh charge advances along the axis of the cylinder, progressively pushing and mixing with the residual gases; it may also reach the exhaust ports, where it is eventually expelled together with residual gas. According to these considerations, and differently from the theoretical perfect mixing model, the fresh charge distribution along the cylinder was not considered uniform and was assumed to depend on the instantaneous flow conditions; on the generic normal section of the cylinder, instead, the fresh charge distribution was assumed be uniform. In the model developed, the two gases involved in the scavenging process, i.e. fresh charge and residual gas, are assumed to remain separated, sharing the same pressure (whose variation propagates at the speed of sound, i.e. almost instantaneously to the whole cylinder volume) but retaining their distinct temperature (whose variation instead does not propagate rapidly) and gas constants, which means also different density, specific heats, etc..: for this reason, the model developed may be considered a two-zones scavenging model. As represented in Fig. 5, the conceived model allows the simultaneous presence of three different situations within the cylinder volume, i.e. a portion with only fresh charge, a portion with a dilution of the two gases, and a portion with residual gas only. Moreover, with the aim to make the model simple to manage, the authors assumed that, in the volume portion where the two gases are simultaneously present, the distribution of each gas varies linearly along the cylinder axis. This assumption has been mathematically implemented into the model by means of the parameter $\chi_a(x)$, defined as the local volumetric fraction of the fresh charge in the cylinder section at the generic position x:

$$\chi_a(x) = \frac{V_a(x)}{V_{tot}(x)} = \frac{V_a(x)}{V_{res}(x) + V_a(x)} \tag{28}$$

As reported in Fig. 5, the coordinate x along the cylinder axis was adopted for the representation of the gas distribution, with the origin ($x = 0$) set at the crown of piston 1 and the end at the crown of piston 2 ($x = L$), being L the total length of the gas cylinder (distance between pistons). It is worth highlighting two particular values of the coordinate x, i.e. the axial position x_1 and x_2 at which the fresh charge concentration starts and stop its linear variation, as shown in Fig. 5; the molar fraction values χ_{a1} and χ_{a2} correspond to the two particular position x_1 and x_2. The situation depicted in Fig. 5 allows distinguishing three different portions of the cylinder volume:

- From the crown of piston 1 to x_1, the fluid is purely fresh charge ⇒ $\chi_a(x) = 1$ for $0 \leq x \leq x_1$.
- From x_1 to x_2 the fresh charge concentration linearly decreases from $\chi_{a1} = 1$ to $\chi_{a2} = 0$.
- From x_2 to L the fluid is composed entirely by residual gases, i.e. $\chi_a(x) = 0$ for $x_2 \leq x \leq L$.

The exhaust ports, whose opening is controlled by the motion of piston 2, is located at the coordinate x_3 and has a variable axial height $h_2(\theta)$; it derives that:

$$L = x_3 + h_2(\theta_2) \tag{29}$$

During the scavenging process, if x_2 reaches the coordinate x_3, the fresh charge starts to be expelled through the exhaust ports.

Indeed, the assumption of a linear variation of the fresh charge concentration along the cylinder axis is a simplified representation of a more complex phenomenon, which may be studied with higher accuracy and detail by means of the more sophisticated tool represented by 3D CFD, but at the cost of calculation times which are order of magnitude higher than the calculation times required by the model here proposed (to give an idea, the average clock time for every complete engine cycle simulated by the proposed model was 21.2 s). Fig. 6 shows some results of 3D CFD simulations performed on the same engine considered in this study [14]: the three pictures refer to three different moments (i.e. at

Table 3
Flow-related parameters.

Parameter	Symbol	Value	Unit
Intake pressure	MAP	1,106-1,200	bar
Exhaust ambient pressure	p_e	1,1	bar
Intake ambient temperature	$T_{a,0}$	350	K
Ports discharge coefficient	C_d	0,7	–

140°, 160° and 180° CA after TDC) and reproduce the in-cylinder dilution between fresh charge (coloured in blue and associated the value of 0 by the included colormap) and residual gas (which instead is represented in red and corresponds to the value of 1).

As can be noted, a diagram is overlapped to each picture, reporting the progress of the residual gas dilution (white dots) along the cylinder, calculated by means of a colour recognizing algorithm expressly developed in MATLAB (intake and exhaust ducts are excluded). It can be noted that in the initial phase of the scavenging process (at 140° CA after TDC, i.e. 40° CA before BDC), the fresh charge is concentrated in the intake side of the cylinder, while only residual gas leaves the cylinder: this situation corresponds to a perfect displacement, as confirmed by the high scavenging efficiency values reported in Fig. 1 for the lower delivery ratios. As shown by the dashed broken line, in this case approximating the residual gas distribution along the cylinder axis by means of a linear approach is not far from real.

Proceeding with the scavenging process, at 160° CA after TDC, a higher fresh charge mass has entered the cylinder and is moving toward the exhaust side; in this situation only residual gas is still flowing away through the exhaust ports; as can be noted, this time the linear approximation depicted by the dashed line has a more marked deviation from the real distribution. In the third picture (referring to 180° CA after TDC, i.e. at BDC) the fresh charge has almost filled the cylinder (the residual gas dilution varies from 0 to 0.13) and the linear approximation represented by the dashed broken line is again near the real distribution.

This brief analysis just carried out on the three pictures reported by reference [14] does not aim at demonstrating the admissibility of the linear approach proposed in this paper, but rather has the meaning to show that the assumption of a linear variation of the residual (and fresh) charge concentration along the cylinder is not too far from the real situation.

2.4.1. Modelling the progressive dilution

The coordinates x_1 and x_2 evolve during the scavenging process as a function of both the fresh charge mass entering the cylinder and the mass leaving through the exhaust ports. The variation of the axial dilution profile is governed by the function $\chi_a(x)$, whose slope between x_1 and x_2 is ψ (normally negative) and represents the linear variation of fresh charge concentration along the cylinder axis. This slope obviously changes during the scavenging process, due to several reasons: it spontaneously tends to zero because of the natural tendency of the two gas to mix uniformly and may be altered by the rate at which in-cylinder mass leaves the cylinder. To account both effects, the evolution of the slope ψ was modelled as function of the crank position:

$$\psi(\theta) = \psi_0 + \phi \cdot \int_{\theta_{i,s}}^{\theta} \frac{G_{out}}{\omega}\, d\theta = \psi_0 + \frac{\phi}{\omega} \cdot \int_{\theta_{i,s}}^{\theta} G_{out}\, d\theta \tag{30}$$

where ψ_0 is the slope initial value and ϕ is a constant parameter that governs the variation of the slope as a function of the mass flowing out from the cylinder during the scavenging phase. $\theta_{i,s}$ is the crank angle at which the inflow begins.

The parameter ψ is re-initialized to its initial value ψ_0 at the beginning of each scavenging event. Eq. (30) therefore governs the evolution of the dilution slope only during the scavenging phase within a given engine cycle, as a function of the cumulative exhaust mass flow rate during that phase.

The instantaneous evaluation of each parameter related to gas distribution inside the cylinder is obtained by the application of the system governing equations, which are:

- Mass conservation
- First law of thermodynamics in differential form
- Ideal gas law

For clarity, the subscript "*a*" refers to quantities associated with the fresh charge zone, "*res*" instead refers to the residual gases, while "*s*" denotes the mixture of fresh charge and residual gas. A secondary subscript "*0*" indicates the initial conditions.

Considering mass conservation, the amount of fresh charger inside the cylinder m_a must corresponds with the difference between the fresh charge entered through the intake ports and the fresh charge left out from the exhaust ports:

$$m_a(\theta) = \int_{\theta_{i,s}}^{\theta} \frac{G_{in} - G_{a,out}}{\omega}\, d\theta \quad \text{where} \quad G_{a,out} = G_{out} \cdot \overline{\chi_{a3L}} \cdot \frac{\rho_a}{\rho_s} \tag{31}$$

Where G_{in} expresses the fresh charge entering the cylinder, G_{out} the mass flowing out, whose portion of fresh charge is indicated as $G_{a,out}$ and is obtained by multiplying for the average concentration of fresh charge in the exhaust flow ($\overline{\chi_{a3L}}$ calculated in Eq. (43)) and for the gas density ratio, being ρ_s the density of the gas mixture at the exhaust ports:

$$\rho_s = \rho_a \cdot \overline{\chi_{a3L}} + \rho_{res} \cdot (1 - \overline{\chi_{a3L}}) \tag{32}$$

Using the perfect gas law, the same fresh charge mass (m_a) inside the cylinder may be related to its temperature T_a, its pressure p and to the volume it takes V_a, through its gas constant R'_a:

$$p \cdot V_a = R'_a \cdot T_a \cdot m_a \tag{33}$$

assuming a uniform pressure in the whole cylinder volume (i.e. $p_a = p_{res} = p$). The same considerations apply to the residual gas mass m_{res}, so that:

$$m_{res}(\theta) = m_{tot}(\theta_{e,o}) - \int_{\theta_{e,o}}^{\theta} \frac{G_{res,out}}{\omega}\, d\theta \quad \text{where} \quad G_{res,out} = G_{out} \cdot (1 - \overline{\chi_{a3L}}) \cdot \frac{\rho_{res}}{\rho_s} \tag{34}$$

being $m_{tot}(\theta_{e,o})$ the total in-cylinder mass when the exhaust ports open (at crank position $\theta_{e,o}$), and $G_{res,out}$ the residual gas flow leaving the cylinder, evaluated as portion of the mass flow out G_{out} by means of the average concentration $\overline{\chi_{a3L}}$ and the gas densities. The mass conservation equations are then completed by the overall mass balance:

$$m_{tot}(\theta) = m_a(\theta) + m_{res}(\theta) \tag{35}$$

where m_{tot} represents the total mass inside the cylinder. The scavenging model equations are combined with the volume related equations:

$$V(\theta) = V_a(\theta) + V_{res}(\theta) \tag{36}$$

$$\frac{\partial V}{\partial \theta} = \frac{\partial V_a}{\partial \theta} + \frac{\partial V_{res}}{\partial \theta} \tag{37}$$

As mentioned before, also the First Law of Thermodynamics, whose general expression is reported in Eq. (10), was employed to properly complete the set of equations necessary to simulate the scavenging process. Its application to the fresh charge mass (m_a) allows computing the in-cylinder pressure:

$$\frac{\partial p}{\partial \theta} = \frac{k_a - 1}{V_a} \cdot \frac{G_{in} \cdot T_{a0} \cdot c_{p,a0} - G_{a,out} \cdot c_{p,a} \cdot T_a}{\omega} - p \cdot \frac{k_a}{V_a} \frac{\partial V_a}{\partial \theta} \tag{38}$$

While the application to the residual gas mass (m_{res}) allows computing the in-cylinder residual gas volume V_{res}:

$$\frac{\partial V_{res}}{\partial \theta} = \frac{1}{p} \cdot \frac{G_{res,out} \cdot c_{p,res} \cdot T_{res}}{\omega} \frac{k_{res} - 1}{k_{res}} - \frac{V_{res}}{k_{res}\, p} \cdot \frac{\partial p}{\partial \theta} \tag{39}$$

The system of equations is closed through the application of the ideal gas law to both gas types. This system of equations captures the evolution of composition and thermodynamic properties along the cylinder axis during the scavenging process, effectively modelling the progressive dilution of residual gases by the incoming fresh charge. As example, Fig. 4 shows the simulated inlet and outlet mass flows as a function of

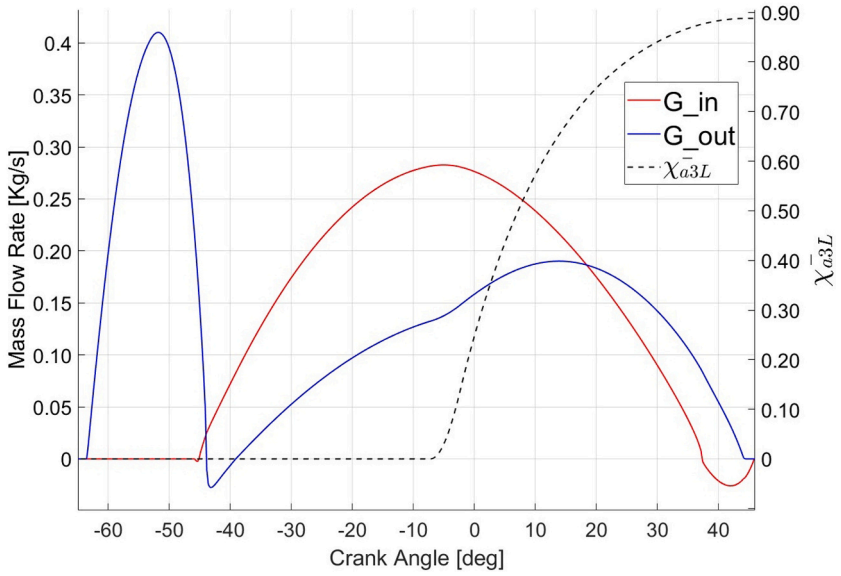

Fig. 4. Inlet and outlet mass flow, comparing with $\overline{\chi_{a3L}}$. (MAP = 1,14 bar, crank angles referred to piston1 BDC).

crank position, together with the average fresh charge concentration evaluated between x_3 and L.

For clarity of presentation, it is worth analysing some generic case that could occur during the scavenging process. The first possible case is represented in Fig. 5, where the fresh charge enters the cylinder, but the dilution front has not yet reached the exhaust ports, i.e. $x_1 \geq 0$ and $x_2 < x_3$. Since $\chi_{a1} = \chi_a(x_1)$ and $\chi_{a2} = \chi_a(x_2)$ represent the fresh charge concentrations at x_1 and x_2 respectively, the volume V_a occupied by the fresh charge mass can be calculated as:

$$V_a = \frac{\pi}{4}\cdot B^2 \cdot x_1 \cdot \chi_{a1} + \frac{\pi}{4}\cdot B^2 \cdot (x_2 - x_1)\cdot \frac{\chi_{a1} + \chi_{a2}}{2} \tag{40}$$

In the case depicted in Fig. 5.

$\chi_{a1} = 1$ and $\chi_{a2} = 0$.

The volume occupied by the fresh charge hence becomes:

$$V_a = \frac{\pi}{4}\cdot B^2 \cdot \left(x_1 + \frac{x_2 - x_1}{2}\right) \tag{41}$$

Combining this formulation with the perfect gas low applied to the fresh charge mass it is possible to find the coordinates x_1 and x_2:

$$\begin{cases} p\dfrac{\pi B^2}{4}\left(x_1 + \dfrac{x_2 - x_1}{2}\right) = m_a T_a R'_a \\ \psi = \dfrac{\chi_{a2} - \chi_{a1}}{x_2 - x_1} = \dfrac{-1}{x_2 - x_1} \end{cases} \Longrightarrow \begin{cases} x_2 = \dfrac{m_a T_a R'_a}{p\dfrac{\pi B^2}{4}} - \dfrac{1}{2\psi} \\ x_1 = x_2 + \dfrac{1}{\psi} \end{cases} \tag{42}$$

The slope ψ is obtained by means of Eq. (30) once the two model parameters ψ_0 and ϕ have been identified.

A second possible case is reported in Fig. 7, where the dilution front exceeds the exhaust port position, i.e. $x_1 < x_3$ and $x_3 \leq x_2 \leq L$. In this case a portion of the fresh charge begins to escape through the exhaust ports.

Also in this case is $\chi_{a1} = 1$ and $\chi_{a2} = 0$

If χ_{a3} indicates the fresh charge concentration χ_a at the axial coordinate x_3 (corresponding to the exhaust port), the outflowing mass of fresh charge can be computed using the average fresh charge concentration between x_3 and L:

$$\overline{\chi_{a3L}} = \frac{\displaystyle\int_{x_3}^{L} \chi_a(x)\, dx}{L - x_3} \tag{43}$$

$$\begin{cases} p\dfrac{\pi B^2}{4}\left(x_1 + \dfrac{x_2 - x_1}{2}\right) = m_a T_a R'_a \\ \psi = \dfrac{\chi_{a2} - \chi_{a1}}{x_2 - x_1} = \dfrac{\chi_{a3} - \chi_{a1}}{x_3 - x_1} = \dfrac{-1}{x_2 - x_1} = \dfrac{\chi_{a3} - 1}{x_3 - x_1} \\ \overline{\chi_{a3L}} = \dfrac{\chi_{a3}(x_2 - x_3)}{2h_2} \end{cases} \rightarrow \begin{cases} x_2 = \dfrac{m_a T_a R'_a}{p\dfrac{\pi B^2}{4}} - \dfrac{1}{2\psi} \\ x_1 = x_2 + \dfrac{1}{\psi} \\ \overline{\chi_{a3L}} = \dfrac{[1 - \psi(x_3 - x_1)](x_2 - x_3)}{2h_2} \end{cases} \tag{44}$$

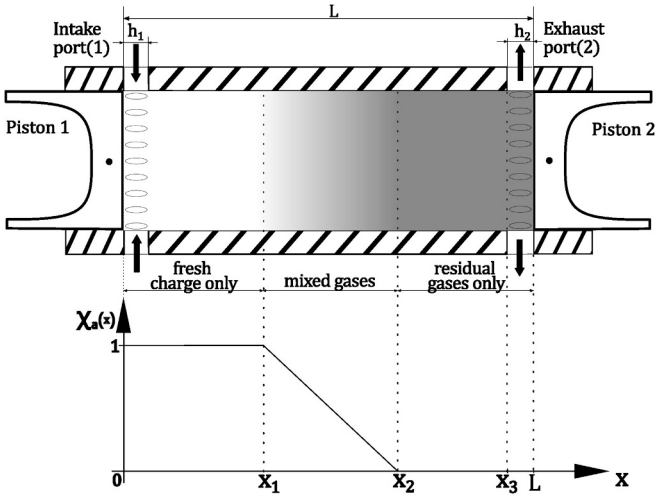

Fig. 5. Schematic representation of the two-zone scavenging model.

Case III: $x_1 < x_3, x_2 = L$

Since x_2 reaches its maximum value, i.e. L, this creates the condition in which $\chi_{a2} > 0$.

In this case the position x_2 is known (=L), hence, as reported in Eq. (45), the fresh charge mass balance is employed to evaluate the concentration χ_{a2}.

The model also allows to face the situation in which the coordinate x_1 exceeds x_3. This may be represented by two alternative configurations to Cases II and III that will be shown here.

Case IIa: $x_1 > x_3$ and $x_1 < x_2 < L$

$$\begin{cases} p\dfrac{\pi B^2}{4}\left(x_1 + \dfrac{x_2 - x_1}{2}\right) = m_a T_a R_a' \\ \psi = -\dfrac{1}{x_2 - x_1} \\ \overline{\chi_{a3L}} = \left[(x_1 - x_3) + \dfrac{x_2 - x_1}{2}\right]\dfrac{1}{h_2} \end{cases} \rightarrow \begin{cases} x_2 = \dfrac{m_a T_a R_a'}{p\dfrac{\pi B^2}{4}} - \dfrac{1}{2\psi} \\ x_1 = x_2 + \dfrac{1}{\psi} \\ \overline{\chi_{a3L}} = \left[(x_1 - x_3) + \dfrac{x_2 - x_1}{2}\right]\dfrac{1}{h_2} \end{cases} \tag{46}$$

Case IIIa: $x_1 > x_3$ and $x_2 = L$

$$\begin{cases} p\dfrac{\pi B^2}{4}\left[x_1 + \chi_{a2}(L - x_1) + \dfrac{(1 - \chi_{a2})(L - x_1)}{2}\right] = m_a T_a R_a' \\ \psi = \dfrac{\chi_{a2} - 1}{L - x_1} = \dfrac{\chi_{a3} - 1}{x_3 - x_1} \\ \overline{\chi_{a3L}} = \dfrac{\chi_{a3} h_2 + \dfrac{(\chi_{a3} - \chi_{a2})h_2}{2}}{h_2} \end{cases} \rightarrow \begin{cases} \chi_{a2} = \dfrac{\dfrac{1}{\psi} + \sqrt{\dfrac{1}{\psi^2} - 4\dfrac{1}{2\psi}\left(\dfrac{1}{2\psi} + L - \dfrac{m_a T_a R_a'}{p\dfrac{\pi B^2}{4}}\right)}}{\dfrac{1}{\psi}} \\ x_1 = L - \dfrac{\chi_{a2} - 1}{\psi} \\ \overline{\chi_{a3L}} = \dfrac{\chi_{a2} + 1 + \psi(x_3 - x_1)}{2} \end{cases} \tag{45}$$

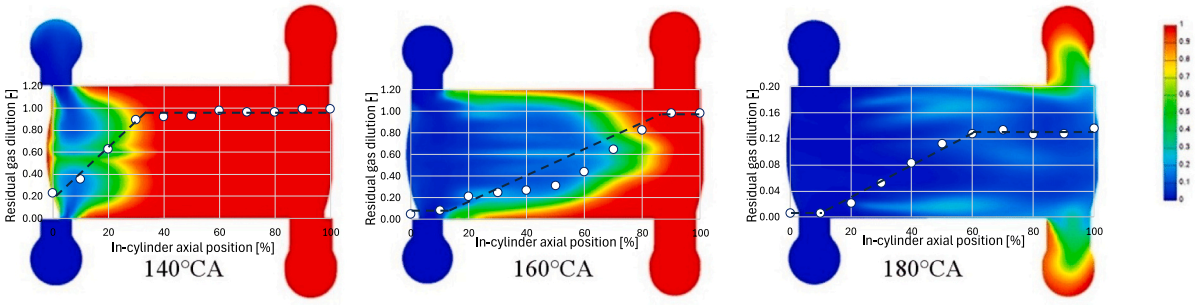

Fig. 6. Residual gas concentration according to CFD 3D results (courtesy of Elsevier, [14]).

$$\begin{cases} p\dfrac{\pi B^2}{4}\left(x_1+\dfrac{L-x_1}{2}\right)=m_aT_aR_a' \\ \psi=\dfrac{\chi_{a2}-1}{L-x_1} \\ \overline{\chi_{a3L}}=\left[(x_1-x_3)+\chi_{a2}(L-x_1)+\dfrac{(1-\chi_{a2})(L-x_1)}{2}\right]\dfrac{1}{h_2} \end{cases} \rightarrow \begin{cases} \chi_{a2}=\dfrac{\dfrac{1}{\psi}+\sqrt{\dfrac{1}{\psi^2}-4\dfrac{1}{2\psi}\left(\dfrac{1}{2\psi}+L-\dfrac{m_aT_aR_a'}{p\dfrac{\pi B^2}{4}}\right)}}{\dfrac{1}{\psi}} \\ x_1=L-\dfrac{\chi_{a2}-1}{\psi} \\ \overline{\chi_{a3L}}=\dfrac{1}{2h_2}\left[x_1+L-2x_3+\chi_{a2}(L-x_1)\right] \end{cases} \tag{47}$$

It must be pointed out that in Fig. 7, Fig. 8, Fig. 9 and Fig. 10, the coordinate x_3 has been intentionally shifted toward the origin to enhance the visualization of the respective cases.

2.4.2. *Chemical composition at the end of the scavenging process*

During the scavenging process, the gas composition inside the cylinder is defined separately for the two zones: in the region occupied by the fresh charge, the fluid is assumed to consist solely of air, modelled as a binary mixture of oxygen and nitrogen with constant mass fractions; in the residual gas zone, instead, the composition reflects that of the working fluid from the previous cycle. At the end of the scavenging phase, when all the ports get closed, it is assumed that the entire cylinder contents undergo instantaneous and complete mixing. The resulting gas composition is therefore computed as a mass-weighted average of the chemical species present in the two contributions: the trapped fresh charge and the residual gases retained in the cylinder. This averaged composition is then used as the initial condition for the subsequent compression phase, providing a coherent link between the scavenging process and the continuation of the thermodynamic cycle.

3. Model Calibration

As shown through the equations describing the scavenging model and the calculation procedure, the values of two parameters are necessary to start the simulation, i.e. ψ_0 and ϕ: the first represent the initial value of the slope of the linear dilution inside the cylinder, while the second account for the slope variation due to mass flowing outside the cylinder. A proper identification of these two parameters is fundamental for a reliable simulation of the scavenging process. A calibration procedure was then carried out by the authors with the aim to allow the model reproducing experimental data related to the scavenging process. For this purpose, reference was made to the experimental data published for the opposed-piston engine developed by the Beijing Institute of Technology [14]. Experimental data points for scavenging efficiency and trapping efficiency as a function of the delivery ratio were used. The scavenging efficiency, denoted as λ_v, is defined as the ratio between the mass of air trapped in the cylinder at the end of the scavenging process and a reference mass, calculated as the product of the air density at the delivery conditions and the swept volume of the cylinder at exhaust and intake ports closure. The delivery ratio, denoted as y, represents the total mass of air that has passed through the cylinder during scavenging, again normalized by the reference mass. Finally, the trapping efficiency η_s represents the efficiency of the scavenging process and is expressed as the ratio between the mass of air trapped in the cylinder and the total mass of air employed for the scavenging: it can be hence evaluated as:

$$\eta_s=\frac{\lambda_v}{y} \tag{48}$$

Fig. 11 reports the experimental data extracted from [14] and employed in this paper for the model calibration.

The quantities of fresh charge that transit through and are trapped in the cylinder during scavenging were calculated using the following integrals:

$$m_{a,trapped}=\int_{\theta_{i,s}}^{\theta_{i,c}}\frac{G_{in}-G_{a,out}}{\omega}d\theta \quad m_{a,scavenged}=\int_{\theta_{i,s}}^{\theta_{i,c}}\frac{G_{in}}{\omega}d\theta \tag{49}$$

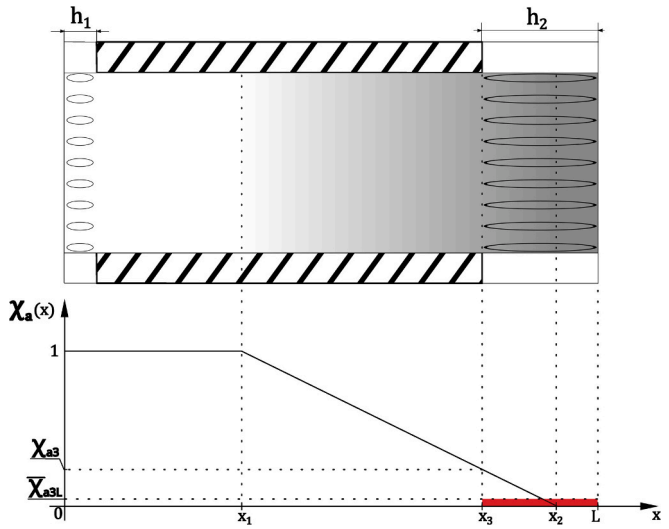

Fig. 7. Scavenging process: Case II.

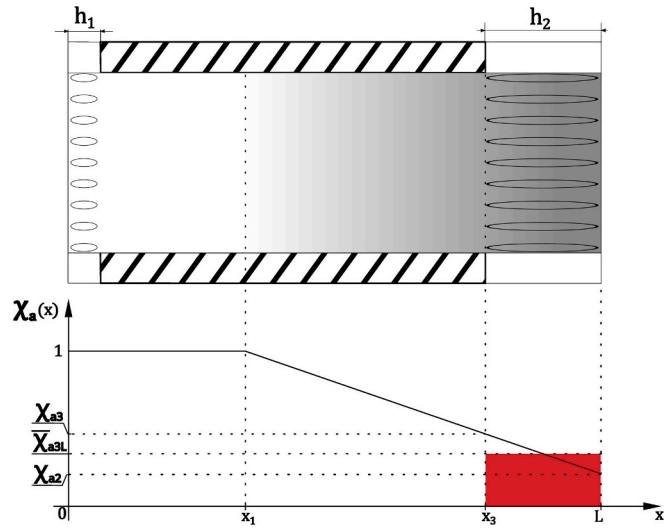

Fig. 8. Scavenging model Case III.

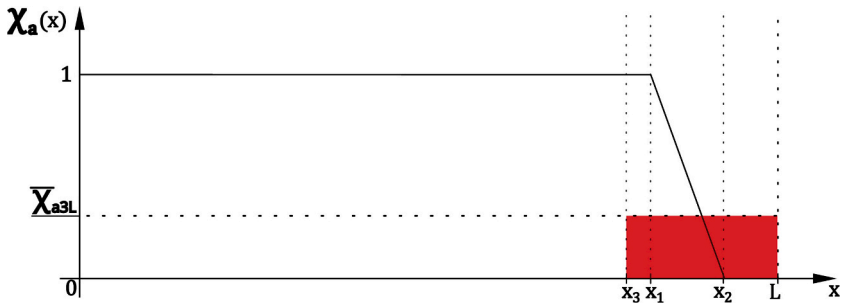

Fig. 9. Scavenging Model Case IIa.

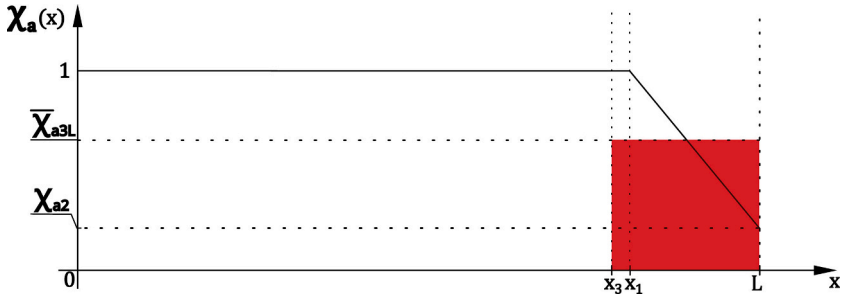

Fig. 10. Scavenging Model Case IIIa.

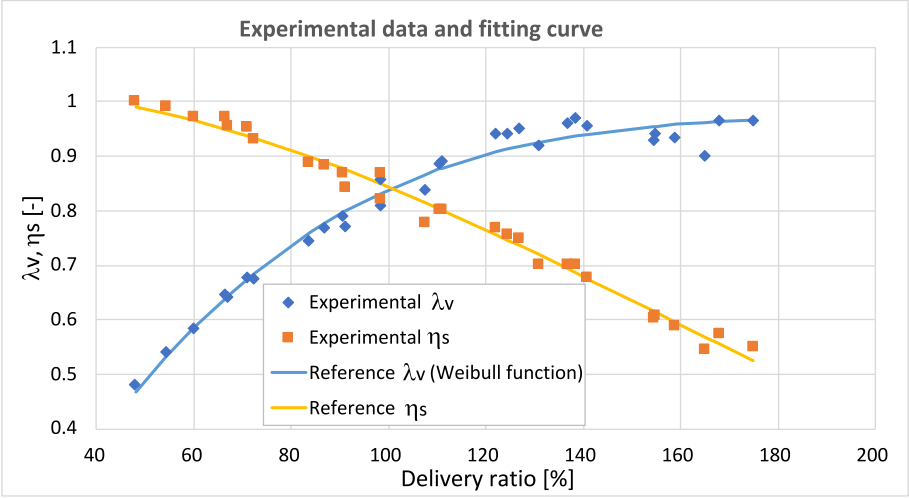

Fig. 11. Experimental data and fitting curve employed for model calibration.

For the calibration of the model, it was necessary to compare the model predicted scavenging and trapping efficiencies with the experimental measured values for the same delivery ratios. Since the model inputs are represented by the boundary conditions (pressure and temperature at inlet, pressure at outlet, engine speed of revolution) and the thermochemical properties of the gas, the delivery ratio cannot be imposed as input parameter, but may only be obtained as an output result of the simulation (it can be calculated once the scavenging process is finished). Performing simulations at different inlet pressure values produces different delivery ratios, which however cannot be identical to the experimental delivery ratios reported for the reference engine [14]. For this reason, the experimental scavenging efficiencies have been interpolated by means of a proper fitting curve, which allowed obtaining a reliable reference value for each delivery ratio obtained by the simulations. Several different mathematical model have been considered and the best agreement was found using a Weibull function (also reported in Fig. 11), which has a mathematical expression similar to the perfect mixing equation:

$$\lambda_v = \alpha - \gamma \cdot e^{(-\delta \cdot y^{\epsilon})} \tag{50}$$

For each delivery ratio, the reference trapping efficiency η_s was calculated from Eq. (48) based on the reference scavenging efficiency obtained by the regression curve of Eq. (50). Table 4 resumes the coefficients of the interpolating function, while Fig. 11 shows the

Table 4
Regression coefficients of the interpolating function.

Parameter	Weibull Model (λ_v)
α	0,97787
γ	0,97549
δ	0,0019647
ϵ	1,4983

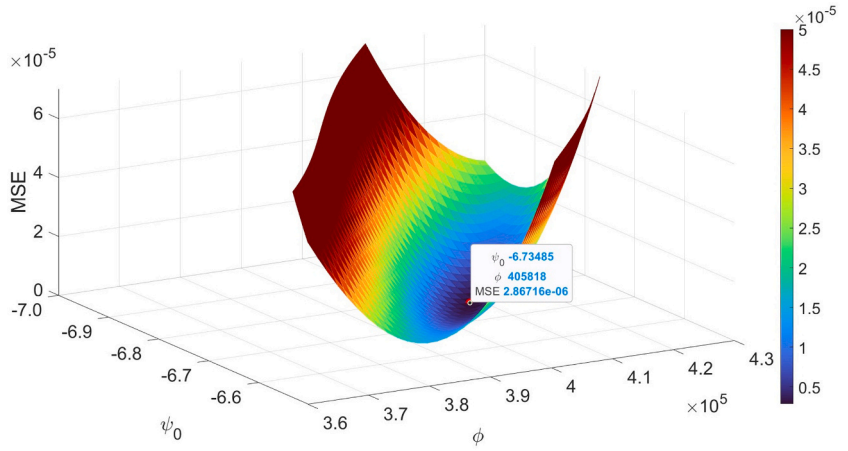

Fig. 12. Colormap of Scavenging efficiency MSE.

experimental values and the reference curve employed for the model calibration.

As highlighted by Y. Liu [14] and shown in Fig. 11, the experimental data exhibit considerable scatter for delivery ratio values exceeding 140%. It is worth noting that the use of a fitting curves for the model calibration procedure allowed also to overcome the inconsistencies deriving from the data dispersion observed in the experimental data.

A further consideration must be made on the calibration based on experimental data from a diesel-fuelled OP2S engine. It may be argued that a different fuel may involve different thermochemical properties or different temperatures of the residual gas, which in turn may affect the scavenging process. The scavenging process, however, is primarily governed by port geometry, piston kinematics and pressure ratios between intake, cylinder and exhaust, while a secondary effect may be played by different residual gas properties or temperatures. Given the operating conditions considered in the paper, the in-cylinder pressure at the beginning of scavenging is comparable across different fuelling strategies, and therefore no major differences in the dominant scavenging dynamics are expected solely due to the residual-gas properties or temperatures. Moreover, the engine cycle simulations were carried out considering a lean air-hydrogen mixture, which implies that the composition of the residual gas obtained by the combustion of hydrogen is not too much different from the residual gas composition obtained by the Diesel combustion of reference [14]. As example, considering a relative air-fuel ratio $\lambda = 1.5$, it would result that the maximum difference in the isentropic coefficient of the two different residual gases would not exceed 1%, while the difference in terms of perfect gas law constant (R' = p v/T) is only 6%.

4. Results

For the model calibration, a parametric analysis was conducted in the (ψ_0, ϕ) space. The parameters were varied within the ranges $\psi_0 \in [-10, -2]$ and $\phi \in [1.4 \bullet 10^5, 7.0 \bullet 10^5]$, each discretized into 12 equally spaced values, yielding a total of 144 combinations. For each couple of parameters (ψ_0, ϕ), a series of simulations were performed considering 10 different values of intake pressure (MAP), generated according to a quadratic increasing law within the interval [1.106 bar, 1.2 bar], with the aim to obtain ten different delivery ratios. Each set of

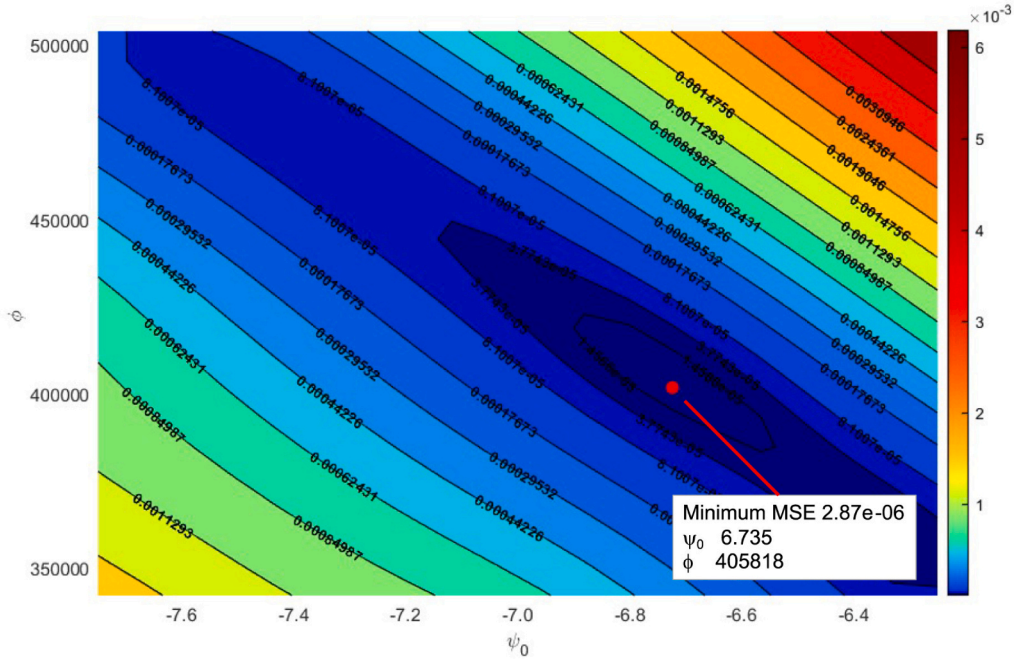

Fig. 13. Contour map of scavenging and trapping efficiency MSE.

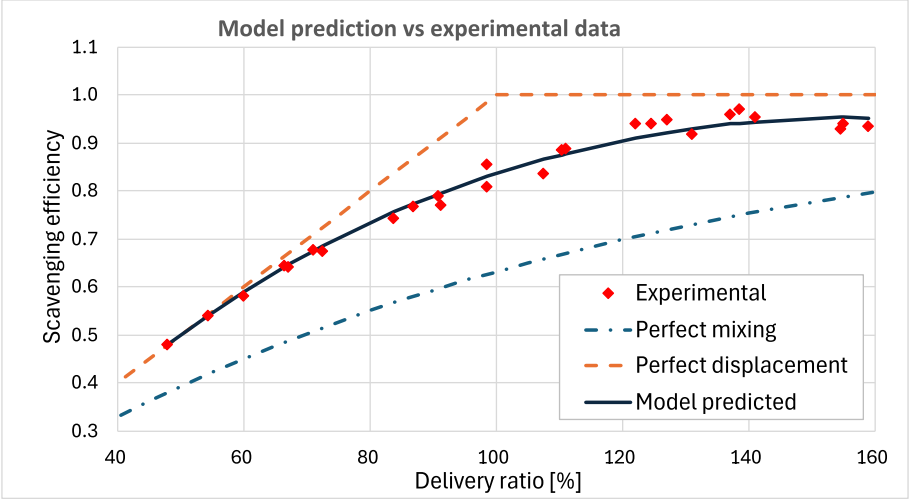

Fig. 14. Scavenging efficiency as function of delivery ratio: comparison between the model prediction and the experimental data.

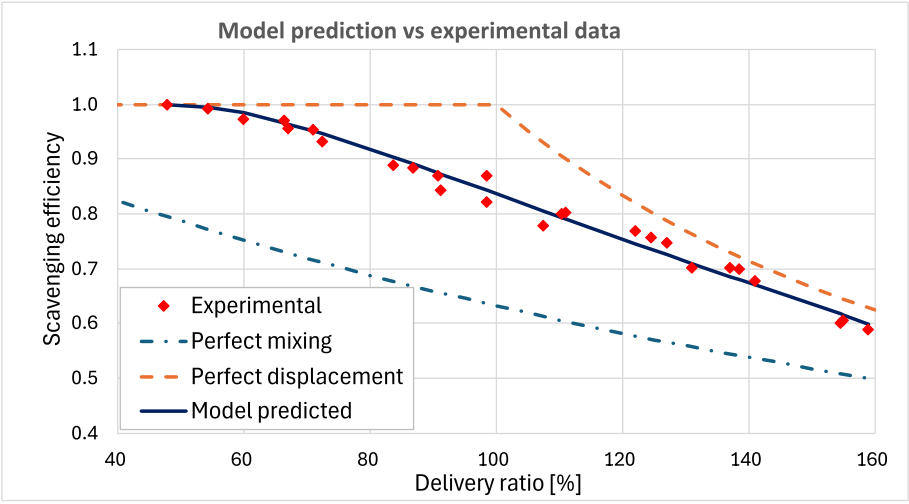

Fig. 15. Trapping efficiency as function of delivery ratio: comparison between the model prediction and the experimental data.

simulation produced a characteristic curve describing the behaviour of the scavenging efficiency and trapping efficiency as a function of the delivery ratio. The non-uniform distribution of MAP values within the specified range was adopted to improve resolution of the scavenging efficiency curve at low delivery ratios. In this interval, even slight changes in MAP caused sharp increases in delivery ratio, thus requiring a denser discretization to accurately capture the model's response. To quantify the model's accuracy with respect to experimental data, the mean square error (MSE) was computed, and the results were visualized as a three-dimensional map over the entire parameter space, as shown in Fig. 12.

As can be observed, the surface obtained showed a clear minimum error region. The minimum MSE was found in correspondence to the parameters value $\psi_0 = -6.735$ and $\phi = 405818$, as also confirmed by the contour map focused on the minimum error region reported in Fig. 13

As mentioned, the minimum MSE was determined comparing the scavenging efficiencies predicted by the proposed model with the scavenging efficiencies resulting from the fitting curve, for the same delivery ratios. A direct comparison between the model outputs and the experimental measurements of reference paper [14] is hence necessary to further appreciate model prediction accuracy; to this purpose, Fig. 14 shows the comparison between the scavenging efficiency evaluated through the model proposed (calibrated by means of the two optimal parameters values) and the experimental values reported in [14]; Fig. 15 instead reports the comparison between model prediction and experimental data in terms of trapping efficiency: as can be deduced by both graphs, a very good agreement was obtained.

Although a very good agreement has been obtained between model prediction and real experimental data, it must be pointed out however that the model calibration was performed on the basis of a single experimental data set referring to a single engine: the validity or reliability of the proposed model in predicting scavenging efficiencies of different engines should be hence properly verified. It is expected that the two free model parameters (ψ_0, φ) may have variations due to different engine geometrical aspects (port areas, bore/stroke ratios, etc..). Understanding the sensitivity of the model parameters to the geometry would require hence the availability of several experimental data set from different engines, characterized by significative geometrical differences.

5. Conclusions

This study focuses on the modelling of the scavenging process in an opposed-piston two-stroke (OP2S) engine. Wide literature research revealed the absence of references concerning the application of one-

dimensional (1D) approaches to the in-cylinder longitudinal (or uniflow) scavenging process, typical of engine geometries characterized by a high stroke-to-bore ratio, such as in OP2S engines. The paper presents an original 1D scavenging model for OP2S engines that couples full thermodynamic cycle calculations. The main characteristic of the model is a linear progressive-dilution scheme adopted to reproduce the fresh charge dilution and penetration inside the cylinder during the mass-exchange (scavenging) process. The model was implemented in MATLAB/Simulink and calibrated by means of experimental data available for a diesel OP2S engine developed at the Beijing Institute of Technology [14]. Overall, the work provides a transparent modelling alternative to perfect-mixing 0D correlations and CFD-intensive workflows by delivering axial scavenging resolution with a compact two-parameter formulation that is directly implementable at system level. The main outcomes are here summarized:

- Thermodynamically consistent initial conditions:
  A complete cycle (compression, combustion, expansion) was simulated to supply consistent pressure and temperature values at the start of the scavenging process.
- Efficient two-parameter formulation
  In the model proposed, the progressive replacement of residual gases by fresh charge is captured by means of only two scalar parameters, the initial value ψ_0 of the linear distribution slope, and the slope variation coefficient ϕ, allowing the model to describe the key features of OP2S scavenging without resorting to three-dimensional CFD.
- Systematic parametric calibration
  144 different combinations of the two calibrating parameters (ψ_0, ϕ) were explored, taking into consideration ten intake-pressure levels each time. The resulting mean square errors (MSE) evaluated both for the scavenging and trapping efficiencies with respect to reference curves, were mapped over the entire parameter space; the minimum global error was obtained with $\psi_0 = -6.735$ and $\phi = 405818$.
- High predictive accuracy at minimal cost
  The calibrated model reproduces the experimental trends of scavenging and trapping efficiencies with very good agreement, while demanding computational resources orders of magnitude lower than full CFD calculations-making it suitable for extensive design sweeps and real-time applications.
- Limitations
  The model has been calibrated through a single set of experimental data; the availability of additional datasets would be useful to extend and confirm its validity and reliability.

In conclusion, the proposed approach offers a practical balance between reliability of the results and computational speed, providing an effective tool for preliminary design, optimisation, and control development of future opposed-piston two-stroke engines.

CRediT authorship contribution statement

Emiliano Pipitone: Writing – review & editing, Writing – original draft, Supervision, Methodology, Formal analysis, Conceptualization. **Marco Giannone:** Writing – review & editing, Writing – original draft, Visualization, Validation, Software, Investigation, Data curation.

Declaration of competing interest

The authors declare that they have no known competing financial interests or personal relationships that could have appeared to influence the work reported in this paper.

Acknowledgement

This research has been supported by the European Union – Next Generation EU - National Sustainable Mobility Center CN00000023, Italian Ministry of University and Research Decree n. 1033— 17/06/2022, Spoke 12, CUP B73C22000760001

Data availability

Data will be made available on request.

References

[1] L. Jansons, L. Zemite, N. Zeltins, I. Geipele, A. Backurs, Green and sustainable hydrogen in emerging European smart energy framework, Latv. J. Phys. Tech. Sci. 60 (1) (2023) 24–38, https://doi.org/10.2478/lpts-2023-0003.
[2] Ling-zhi Bao, Bai-gang Sun, Qing-he Luo, Optimal control strategy of the turbocharged direct-injection hydrogen engine to achieve near-zero emissions with large power and high brake thermal efficiency, Fuel 325 (2022) 124913, https://doi.org/10.1016/j.fuel.2022.124913.
[3] S. Caprioli, A. Volza, E. Mattarelli, C.A. Rinaldini, High Performance and near Zero Emissions 2-Stroke H2 Engine, SAE Technical Paper 2023-24-0068, 2023, https://doi.org/10.4271/2023-24-0068.
[4] J.-P. Pirault, M.L. Flint, Opposed piston engines: evolution, use, and future applications, SAE International, 2009, https://doi.org/10.4271/R-378.
[5] S. Naik, D. Johnson, J. Koszewnik, L. Fromm, et al., Practical Applications of Opposed-Piston Engine Technology to Reduce Fuel Consumption and Emissions, SAE Technical Paper 2013-01-2754, 2013, https://doi.org/10.4271/2013-01-2754.
[6] G. Regner, D. Johnson, J. Koszewnik, E. Dion, et al., Modernizing the Opposed Piston, Two Stroke Engine for Clean, Efficient Transportation, SAE Technical Paper 2013-26-0114, 2013, https://doi.org/10.4271/2013-26-0114.
[7] F. Redon, C. Kalebjian, J. Kessler, N. Rakovec, et al., Meeting Stringent 2025 Emissions and Fuel Efficiency Regulations with an Opposed-Piston, Light-Duty Diesel Engine, SAE Technical Paper 2014-01-1187, 2014, https://doi.org/10.4271/2014-01-1187.
[8] R. Herold, M. Wahl, G. Regner, J. Lemke, et al., Thermodynamic Benefits of Opposed-Piston Two-Stroke Engines, SAE Technical Paper 2011-01-2216, 2011, https://doi.org/10.4271/2011-01-2216.
[9] G. Regner, R. Herold, M. Wahl, E. Dion, et al., The Achates power opposed-piston two-stroke engine: performance and emissions results in a medium-duty application, SAE Int. J. Engines 4 (3) (2011) 2726–2735, https://doi.org/10.4271/2011-01-2221.
[10] M. Sweeney, G. Swann, R. Kenny, G. Blair, Computational Fluid Dynamics Applied to Two-Stroke Engine Scavenging, SAE Technical Paper 851519, SAE International, Warrendale, PA, 1985, https://doi.org/10.4271/851519.
[11] Blair. G, (1996), Design and Simulation of Two-stroke Engines, SAE International, doi:https://doi.org/10.4271/R-161.
[12] G.P. Blair, The Basic Design of Two-Stroke Engines, Reprint ed., SAE International, Warrendale, PA, 2020 (ISBN 978-1560910084.).
[13] F. Ma, W. Yang, Y. Wang, J. Xu, Y. Li, Experimental research on scavenging process of opposed-piston two-stroke gasoline engine based on tracer gas method, Int. J. Engine Res. (2021), https://doi.org/10.1177/14680874211036613.
[14] Y. Liu, F. Zhang, Z. Zhao, et al., Study on the synthetic scavenging model validation method of opposed-piston two-stroke diesel engine, Appl. Therm. Eng. 104 (2016) 184–192, https://doi.org/10.1016/j.applthermaleng.2016.03.094.
[15] G.P. Merker, M. Gerstle, Evaluation on two stroke engines scavenging models, SAE Trans. 106 (1997) 604–627. http://www.jstor.org/stable/44730705.
[16] D. Dang, F.J. Wallace, Some single zone scavenging models for two-stroke engines, Int. J. Mech. Sci. 34 (1992) 595–604, https://doi.org/10.1016/0020-7403(92)90057-N.
[17] N.P. Kyrtatos, I. Koumbarelis, A three-zone scavenging model for two-stroke uniflow engines, J. Eng. Gas Turb. Power 110 (1988) 531–537, https://doi.org/10.1115/1.3240167.
[18] D. Liu, X. Han, L. Liu, X. Ma, Investigation of the scavenging process in two-stroke uniflow scavenging marine engines by a real-time multi-stage model, Front. Energy Res. 10 (2022) 969525, https://doi.org/10.3389/fenrg.2022.969525.
[19] F. Baudequin, P. Rochelle, Some scavenging models for two-stroke engines, Proc. Inst. Mech. Eng., Part D: Automobile Eng. 194 (1980) 203–210.
[20] Y. Zhou, X. Li, S. Ding, S. Zhao, K. Zhu, L. Shao, F. Du, G. Wang, Z. Xu, Technologies and studies of gas exchange in two-stroke aircraft piston engine: a review, Chin. J. Aeronaut. 37 (1) (2024) 24–50, https://doi.org/10.1016/j.cja.2022.08.012.
[21] Y. Qiao, X. Duan, K. Huang, et al., Scavenging ports' optimal Design of a two-Stroke Small Aeroengine Based on the Benson/Brandham model, Energies 11 (10) (2018) 2739, https://doi.org/10.3390/en11102739.
[22] Xinyan Wang, Hua Zhao, (2019), A High-Efficiency Two-Stroke Engine Concept: The Boosted Uniflow Scavenged Direct-Injection Gasoline (BUSDIG) Engine with Air Hybrid Operation, Engineering, Volume 5, Issue 3, Pages 535-547, ISSN 2095–8099, doi:https://doi.org/10.1016/j.eng.2019.03.008.

[23] F. Ma, L. Zhang, T. Su, Simulation modeling and optimization of Uniflow scavenging system parameters on opposed-piston two-stroke engines, Energies 11 (4) (2018) 940, https://doi.org/10.3390/en11040940.
[24] A. Alqahtani, M. Wyszynski, P. Mazuro, H. Xu, Evaluation of the effect of variable compression ratios performance on opposed piston 2-stroke engine, Combust. Engines 171 (4) (2017) 97–106, https://doi.org/10.19206/CE-2017-417.
[25] F. Ma, C. Zhao, Z. Zhao, S. Zhang, Scavenge flow analysis of opposed-piston two-stroke engine based on dynamic characteristics, Adv. Mech. Eng. 7 (4) (2015), https://doi.org/10.1177/1687814015581569.
[26] E. Mattarelli, S. Caprioli, T. Savioli, A. Volza, C.M. Di Gaetano Iftene, C. A. Rinaldini, Virtual development of a single-cylinder hydrogen opposed piston engine, Energies 17 (21) (2024) 5262, https://doi.org/10.3390/en17215262.
[27] Z. Xie, Z. Zhao, Z. Zhang, Numerical Simulation of an Opposed-Piston Two-Stroke Diesel Engine, SAE Technical Paper 2015-01-0404, 2015, https://doi.org/10.4271/2015-01-0404.
[28] W. Yang, X.-R. Li, Y.-N. Kang, H. Zuo, F.-S. Liu, Evaluating the scavenging process by the scavenging curve of an opposed-piston, two-stroke (OP2S) diesel engine, Appl. Therm. Eng. 147 (2019) 336–346, https://doi.org/10.1016/j.applthermaleng.2018.10.095.
[29] C.R. Ferguson, A.T. Kirkpatrick, Internal Combustion Engines: Applied Thermosciences, 3rd ed., John Wiley & Sons, Hoboken, NJ, 2016.
[30] G. Woschni, A Universally Applicable Equation for the Instantaneous Heat Transfer Coefficient in the Internal Combustion Engine, SAE Technical Paper 670931, SAE International, Warrendale, PA, 1967, https://doi.org/10.4271/670931.
[31] U.S. Department of Commerce, NIST Chemistry WebBook, National Institute of Standards and Technology, http://webbook.nist.gov/chemistry/.